THE ASTROPHYSICAL JOURNAL, 386:106–119, 1992 February 10

FOKKER-PLANCK MODELS AND GLOBULAR CLUSTER EVOLUTION: THE PROBLEM OF M71

G. A. DRUKIER, G. G. FAHLMAN, AND H. B. RICHER
Department of Geophysics and Astronomy, University of British Columbia, Vancouver, B.C., Canada, V6T 1Z4
Received 1991 February 28; accepted 1991 August 19

ABSTRACT

Comparisons are made between star-count mass functions and surface density profiles for the globular cluster M71 and multimass, tidally truncated Fokker-Planck simulations reheated by three-body binaries. The degree of mass segregation and the short relaxation time observed for the cluster suggest that M71 should be a post–core-collapse cluster. In the standard models, the tidal boundary and the degree of mass segregation were approximately reproducible. However, we note that the inferred tidal radius, about 10 pc, is distinctly less than that based on consideration of the cluster's Galactic orbit. On the other hand, while the central surface density profiles are somewhat more concentrated than a King model, the post–core-collapse model surface density profiles are too steep to match these observations. It is shown that gravothermal oscillations are unlikely to affect the comparison between observations and theory except in the case of clusters with extreme cusps. The presence of massive stellar remnants (black holes) can flatten the post–core-collapse surface brightness profile, but such models fail to reproduce the observed mass segregation and also predict an unacceptably high value for the central velocity dispersion. Models in which the heating rate is artificially enhanced do seem to be able to reproduce the observations but, in the absence of an identified source for this extra heating, such models are not physically justified. Thus, it appears that this type of Fokker-Planck model, in which post–core-collapse expansion is driven solely by three-body binaries, is incomplete and that additional physics, such as the effects of stellar evolution or primordial binaries, is required.

Subject headings: celestial mechanics, stellar dynamics — globular clusters: individual (M71) — stars: statistics

1. INTRODUCTION

With the increasing sophistication of Fokker-Planck models for globular cluster evolution has come the ability to make specific comparisons with observations. In particular, we may attempt to match observed properties for a given globular cluster with a selected model. Several papers have recently attempted to match Fokker-Planck simulations with the surface brightness profiles of specific collapsed-core globular clusters. Grabhorn et al. (1991), for example, compare their models to surface brightness profiles and velocity dispersions for M15 and NGC 6624. In any comparison between models (where the stars are classed by mass) and observable quantities (where only the luminosities are known) mass-to-light ratios are required. In the case of the post–main-sequence stars which dominate a cluster's light profile, these can be very uncertain. When the observable quantity is based on star counts, the uncertainties in the post–main-sequence mass-to-light ratios are less important since the numbers are dominated by less-evolved stars. For the same reason, surface brightness profiles provide a poor constraint on the mass function. Larger data sets, preferably based on star counts, are required in order that more detailed tests of the models may be performed. One sign of dynamical evolution is mass segregation in which transfers of energy between stars of different masses have resulted in a settling of the more massive components into the center of the cluster, enhancing the numbers of less massive stars in the halo. Tidal stripping will selectively remove the stars which venture farthest from the core of the cluster, specifically the least massive component, for clusters whose orbits take them deep into the Galactic potential. Lee, Fahlman, & Richer (1991, hereafter LFR), for example, have suggested that a flattened or inverted mass function in the central region is a sign of a highly evolved cluster. The main advantage of using such a cluster is that the results depend less on the initial conditions than in the case where little evolution has taken place. In addition, more of the input physics, especially the nature of the heating source powering the post–core-collapse evolution may be probed. Tests of the models using clusters other than those in deep core collapse will also provide information on the cluster system as a whole, enabling us to address questions such as survival rates for various sets of initial conditions and the relationship between the Galactic halo and the globular cluster system.

In this paper we compare post–core-collapse Fokker-Planck models, driven by three-body binary heating, to the globular cluster M71. This cluster shows a highly flattened mass function, inverted in the core, significant mass segregation (Richer & Fahlman 1989, hereafter RF89), and a peculiar surface density profile. The observational aspects will be discussed in § 2 and the details of the Fokker-Planck models in § 3. The initial comparison in § 4 reveals an inconsistency between the observations and the models. Various attempts to resolve this contradiction are discussed in § 5. The conclusions of this paper are summarized in § 6.

2. OBSERVATIONAL DATA

Detailed star counts in M71 are given in RF89 and are based on a series of overlapping *UBV* CCD frames, which completely cover the central part of the cluster (see Richer & Fahlman 1988). From these data, it was clear that the stars in M71 display a significant degree of mass segregation, broadly consistent with the predictions of a King-Michie model only if a substantial population of low-mass stars were present in the cluster. Subsequent deep observations in a field located some 3′ from the cluster center provided direct evidence of these low-

TABLE 1

SURFACE DENSITY PROFILES

	$12 \le V \le 18$		$18 \le V \le 20$	
r_e (pc)	N (pc^{-2})	±	N (pc^{-2})	±
0.183..........	196.	27.	417.	38.
0.316..........	216.	30.	326.	38.
0.448..........	155.	18.	318.	29.
0.568..........	133.	15.	295.	27.
0.675..........	153.	18.	253.	23.
0.804..........	108.	12.	219.	15.
0.955..........	94.0	8.7	217.	15.
1.135..........	70.0	6.5	217.	15.
1.349..........	64.9	6.0	157.	11.
1.607..........	48.3	3.3	133.	6.
1.910..........	34.0	3.9	108.	7.
2.270..........	25.9	3.0	78.4	5.4
2.698..........	18.1	2.9	51.3	4.7
3.214..........	7.69	2.34	31.4	4.4

mass stars (Richer et al. 1990). The data discussed here are drawn from both of the above sources.

The realization, arising from the LFR study, that M71 could well be in an advanced postcollapse phase of its dynamical evolution, prompted us to reexamine the star counts described in RF89 with a finer spatial grid. The point was to see just how well the counts fit a King model profile, particularly in the central parts of the cluster. The revised star counts are presented in Table 1. In this Table, r_e is the effective radius for the counts; i.e., the radius which bisects the area of the annulus in which the stars are counted (note that the first annulus is, in fact, a circle), N is the number of stars per square parsec in the indicated magnitude range, and the error estimate is based on Poisson statistics. Small completeness corrections were applied to the stars between $V = 19$ and 20 only (see RF89). A distance of 3.68 kpc based on the distance modulus and reddening of Richer & Fahlman (1988) was used in converting the angular dimensions of the observations to the physical dimensions of the models.

The numbers presented here differ slightly from tnose of RF89 for three reasons. (1) The photometry from the long and short exposures was combined in a different way. Here, the photometry lists from the short frames were truncated at $V = 19.0$ prior to merging with the corresponding lists from the long exposure frames. This avoids the need to consider completeness corrections in the short-exposure frames. (2) The overlap between fields was handled differently. For this study we trimmed the frames to provide a seamless fit with no overlap. This avoids the need to consider joint completeness criteria in the overlap area. (3) The adopted center of the cluster is different. In RF89 the cluster center was determined by the centroid of smoothed isopleths obtained from the raw star counts. The center turned out to be located 1''2 E and 5''1 N of the center adopted by Cudworth (1985), which, for convenience, was located on a particular star. Cudworth's central star, in turn, is located 7'' W and 2'' N of the center determined by Shawl & White (1986), which was based on the large scale symmetry of the integrated light. For this study, we redetermined the center by finding the centroid of all the stars in the range $V = 12.0$–19.0, and within a radius of about 1'5 of the cluster center. Starting with the RF89 center, we iterated until a self-consistent center was found. The center adopted here is 5''0 W and 1''4 N of the Shawl-White center. It should be noted that the center at this position is defined by the total number of stars and is not coincident with the centroid of the light emitted by the stars. Our result is, we believe, a better estimate of the center of mass for the cluster. In practice, the surface density profiles obtained around the Shawl-White center do not differ significantly from the results given in Table 1.

The surface density profiles (SDPs) are plotted in Figure 1*a*. In Figure 1*b* the data are shown together with curves from an isotropic, multimass King model. The input mass function for the model was taken from RF89 and includes a bin at 0.1 $M_\odot$ which contains 50% of the total stellar mass. The model shown has a central potential of $W_0 = 4.0$ and the scale radius, $r_s =$ 1'88 (2.01 pc) and vertical normalization were determined by a fit to the counts for stars with $18 < V < 20$. Evidently, the model fit for this bin is quite acceptable. However, the counts of the brighter stars, $12 < V < 18$, show a much higher degree of central concentration than expected from the model. This behavior is typical of a range of models which differ only in W_0. The upper points in Figure 1 are the total counts (offset vertically by 0.5 dex for clarity), also overlaid with the corresponding model curve in Figure 1*b*. The central deviation from the King model, due to the brighter stars, is still evident, but, clearly, the departure is small. The result of this comparison is then inconclusive; there is no evidence for a strong density cusp at the center of M71, but nevertheless, the King models cannot account for the detailed central behavior of the SDPs.

The stellar mass functions (MFs) relevant to this study are shown in Figure 2. The one labeled "core" is based on the RF89 star counts, but a new, oxygen enhanced, mass-luminosity relationship of D. A. VandenBerg (private communication; see Richer et al. 1990) has been used. The second mass function was determined from the deep luminosity function obtained in the 3' field mentioned above and is described in Richer et al. (1990). The mean radius of this field lies at the same distance from the center of the cluster as the outermost point on the SDPs in Figure 1. A calculation of the surface densities in this field for the two mass ranges used in the SDPs gives good agreement with the earlier observation.

As noted by RF89, M71 shows clear signs of mass segregation. The two mass functions shown in Figure 2 highlight this. For stars more massive than 0.6 $M_\odot$ the core MF is inverted while the outer MF is flat. The outer field has a steep increase in number per unit mass as the mass per object decreases from 0.5 $M_\odot$. The core MF is much flatter over the more limited range observed. Both MFs show much more detail than is expected from a simple combination of power laws, and it should not be expected that exact fits to the observations can be made without some fine-tuning of the IMF. Our objective here will be to fit the shapes of the SDPs and the general trends of the MFs. In particular, the drop off in the SDPs beyond 1 pc will give the tidal radius and the gradually sloped interiors will be used in determining the evolutionary phase. The degree of mass segregation will also play an important role in deciding what time of the model best fits the observations.

3. NUMERICAL MODELS

The numerical models employed in this study are based on the isotropic, orbit-averaged form of the Fokker-Planck equation using techniques introduced by Cohn (1980). The actual code used is a descendant of Cohn's but has been extensively modified and added to by a number of people in the past decade. A brief review of the methodology and background

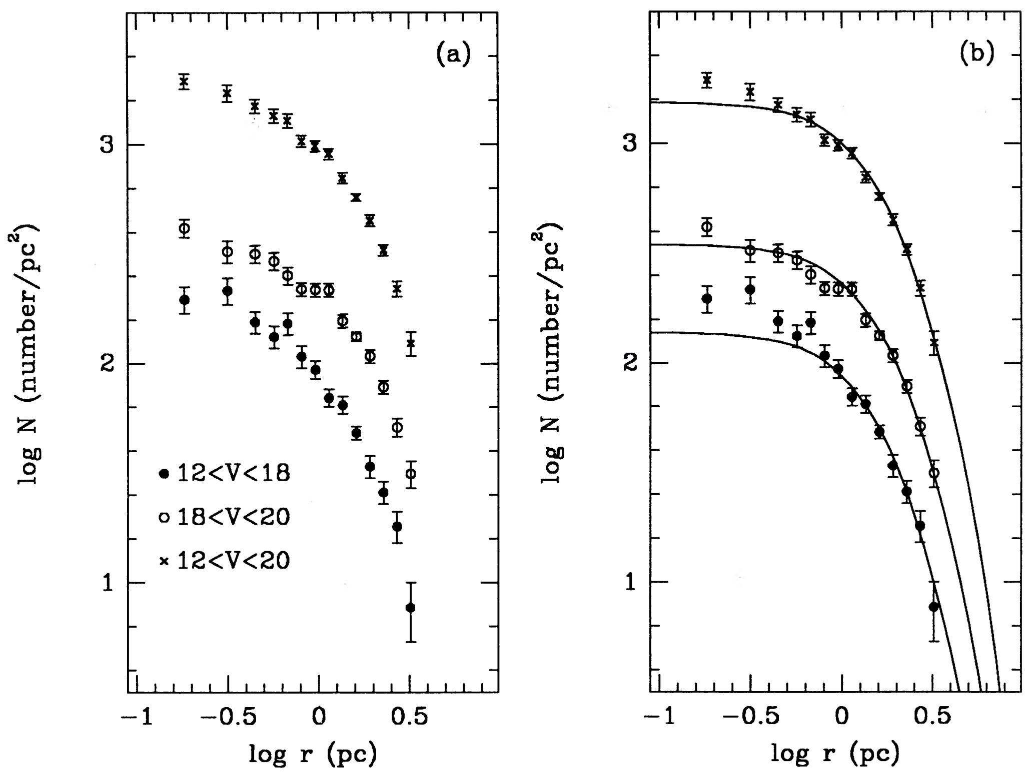

FIG. 1.—(*a*) The surface density profiles for the two most luminous mass classes observed in M71. The filled circles are for stars in the mass interval $0.85 < M/M_\odot < 0.89$, while the open circles are for stars in the mass interval $0.71 < M/M_\odot < 0.85$. These are based on the star counts of RF89 but newly calculated on a finer grid of annuli. The crosses are the sum of the counts over both intervals displaced upward by 0.5 dex for clarity. (*b*) The same data as in (*a*) shown with an isotropic, multimass King model. The radial and density scales were fitted to the less luminous mass class. The more luminous class shows a higher degree of concentration than expected in the model.

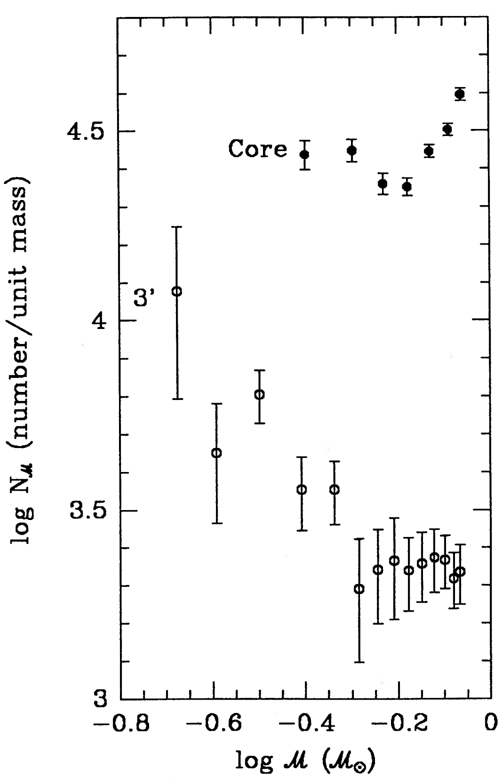

FIG. 2.—Mass functions observed for M71. The filled circles are from RF89 for the inner 3.66 pc of the cluster (core field). The open circles are from Richer et al. (1990) for a rectangular field with mean distance of 3.2 pc (3′ field).

assumptions is therefore in order. As in the original models, the distribution function is held to be a function of the total energy per unit mass and to evolve with time subject to equation (6) of Cohn (1980). For the multimass case, individual distribution functions are used for each mass class, and the diffusion and advection coefficients depend on the mass bin involved. The coefficients used are taken from LFR. In this technique, it is assumed that the cluster is spherically symmetric and that the time scale of the dynamical evolution is much longer than the orbital time of stars within the cluster. Following this approach, all quantities are calculated on an orbit-averaged basis since individual stars travel through the region of the cluster accessible to them several times before they are significantly affected by two-body relaxation. In addition, it is assumed that, unlike the form of the Fokker-Planck equation used in Cohn (1979), the velocity distribution is isotropic so that the distribution function is independent of angular momentum. A two-step, operator splitting technique is used in numerically solving the coupled equations. First, the distribution function is evolved forward in time using the Fokker-Planck equation, while the potential is held fixed. At this point the potential, as found by solving Poisson's equation, is no longer consistent with the distribution function. The second step is thus to recalculate the potential subject to the constraint that the distribution function remain a constant function of the orbit-averaged radial action q (see eq. [4] of Cohn 1980), an adiabatic invariant for small changes in the potential.

Several additional processes have been added to Cohn's bedrock code. These are heating due to the formation and destruction of three-body binaries; tidal stripping by a constant external potential; and a spectrum of stellar masses. The binary heating mechanism is included to reverse the course of core collapse and to power the post–core-collapse evolution. The problem has three dimensions, and since it is convenient to do the calculations in a dimensionless form, three scaling parameters are available. The inclusion of binary heating requires that the total mass of the cluster be specified in order that the relative sizes of the heating and diffusion coefficients be correct and it is useful to choose the units such that $G = 1$. Thus the only free scaling parameter for the dimensionless models is the length scale. The choice of length scale affects the time and velocity scales when comparing the models to observations.

The numerical technique used in calculating the heating rates is that described by Lee (1987) and extended to multiple masses by LFR. The binary stars that heat the cluster are not represented by a distribution function but are treated in a purely statistical manner since very few are expected to be present in the cluster at any given time. The form used here is not the same as that used by Murphy, Cohn, & Hut (1990) but is more consistent with the assumptions made both in that paper and in LFR. The differences between the two approaches are discussed in the Appendix. The effects of tidal stripping were applied following the prescription of Lee & Ostriker (1987). The density of stars in the distribution function at energies below a cutoff corresponding to the tidal boundary is reduced following an exponential law with time constant depending on the energy. Note that the form for the stripping rate given in Lee & Ostriker (1987) is off by a factor of $4\pi^2$ and that of LFR is correct.

It is common in papers reporting Fokker-Planck calculations that the initial form of the model be taken to be Plummer's model. However, since we wished to investigate the effects of initial concentration on the simulation, the initial model has been taken to be a King (1966) model with a given value for the central potential parameter, W_0, and scale radius, with all species having the same initial velocity dispersion. Since it is expected that after the initial gas cloud fragments into stars violent relaxation will take place (Elson, Hut, & Inagaki 1987), leaving stars of all masses with the same velocity dispersions, such an initial model is reasonable.

Apart from some noted exceptions, in all the models discussed here, the main sequence was represented by 10 mass classes covering stars with masses ranging between 0.16 and 0.89 $M_\odot$. The low-mass cutoff was somewhat arbitrary in that it was the low-mass limit to the VandenBerg isochrone used. The Richer et al. (1990) mass function of M71 is still rising sharply at 0.2 $M_\odot$, and we note that the mass function of NGC 6397 has now been observed down to 0.12 $M_\odot$ (Fahlman et al. 1989), indicating that even lower mass stars are present in globular clusters. The model mass function could be extended to even lower masses, but mass segregation makes them unimportant to the dynamics of the core of the model. One model, to be discussed in § 5.2, which was calculated with an additional low-mass bin that extended the low-mass cutoff to 0.1 $M_\odot$, supports this. The mass bins for the higher mass stars were chosen to be the same as the observational bins for the core MF. In addition, three bins were used to represent a distribution of white dwarf stars with masses from 0.9 to 1.14 $M_\odot$. The three white dwarf bins were of equal width, and an equal number of stars was put in each, making up a predetermined number fraction of the stars in the cluster. The main-sequence stars were distributed as a superposition of two power laws. Recent observations have clearly shown that observed mass functions for many globular clusters are poorly represented by single power laws, showing a change in slope near 0.4 $M_\odot$ (Richer et al. 1990). This behavior is seen in the mass functions of M71. In view of these observations, a combination of two power laws, while still an approximation, may be closer to the truth than a single power law. Undoubtedly, the true shape of the IMF is yet more complicated.

Once a set of mass bins has been decided on, a model run is characterized by eight parameters: the slopes of the two power-law mass functions; their relative proportions; and the number fraction of white dwarfs (these four specify the IMF); the central potential parameter W_0 of the King model, which gives the initial distribution function; the initial tidal radius, which gives the scaling; the total mass, which sets the rate constant for the binary heating; and the tidal stripping time scale. Since the relative time scales are independent of the length scale, the tidal radius need not be specified initially and may be varied afterward to improve the fit to observations. The tidal stripping time scale was set equal to the orbital period of the model in the spherical external potential. In the dimensionless units of the model, this provides the almost instantaneous removal of unbound stars. Consideration of the numerical code as we first received it from H. M. Lee indicated that the transformation to dimensionless form required for consistency with the Fokker-Planck formalism used had not been done. For the models described in Lee & Ostriker (1987), this leads to an underestimate of the tidal stripping rate by a factor of 173. Faster tidal stripping and more rapid disruption by the Galactic tidal field are to be expected than that inferred from Lee & Ostriker. These changes were incorporated in LFR.

During each run, the full description of the status of the model was periodically saved for later analysis. For each of these times the process of observation was simulated with the density distributions being projected and the number of stars over appropriate regions (corresponding to the observed CCD fields) integrated. Since the observations have been corrected for the effects of incompleteness and field contamination, these effects were not applied to the models. The SDPs were compared to annular sums over the same annuli as were used for the observations. The model core MF was integrated over a circular area of radius 3.66 pc. The model outer MF was integrated over a rectangular area with the same dimensions and position as that used by Richer et al. (1990). The areas covered by the two MFs overlap to a certain extent, but the core MF is dominated by the higher density of stars in the core of the cluster.

4. STANDARD MODELS

Figure 3 shows the results of a typical run which will be referred to as the "standard run." The initial model was a $W_0 = 4$ King model with total mass $3 \times 10^5\ M_\odot$ and the IMF given in Table 2. The initial tidal radius was taken to be 21.6 pc. The IMF consisted of two power laws with slopes 0.5 and 5.0 (where the Salpeter value is 1.35), with a number ratio of 1:5 and 1% by number distributed equally across the three white dwarf bins. The steep slope of 5 was required in order to match the low mass end of the observed IMF in the 3′ field. Other choices for the IMF are discussed in § 5.2. In Figure 3 the observations as discussed in § 2 are shown with their associated error bars. The model profiles are shown at four times. The dot-dash line shows the initial model, the thick line, the model at the reversal of core collapse, and during the post-

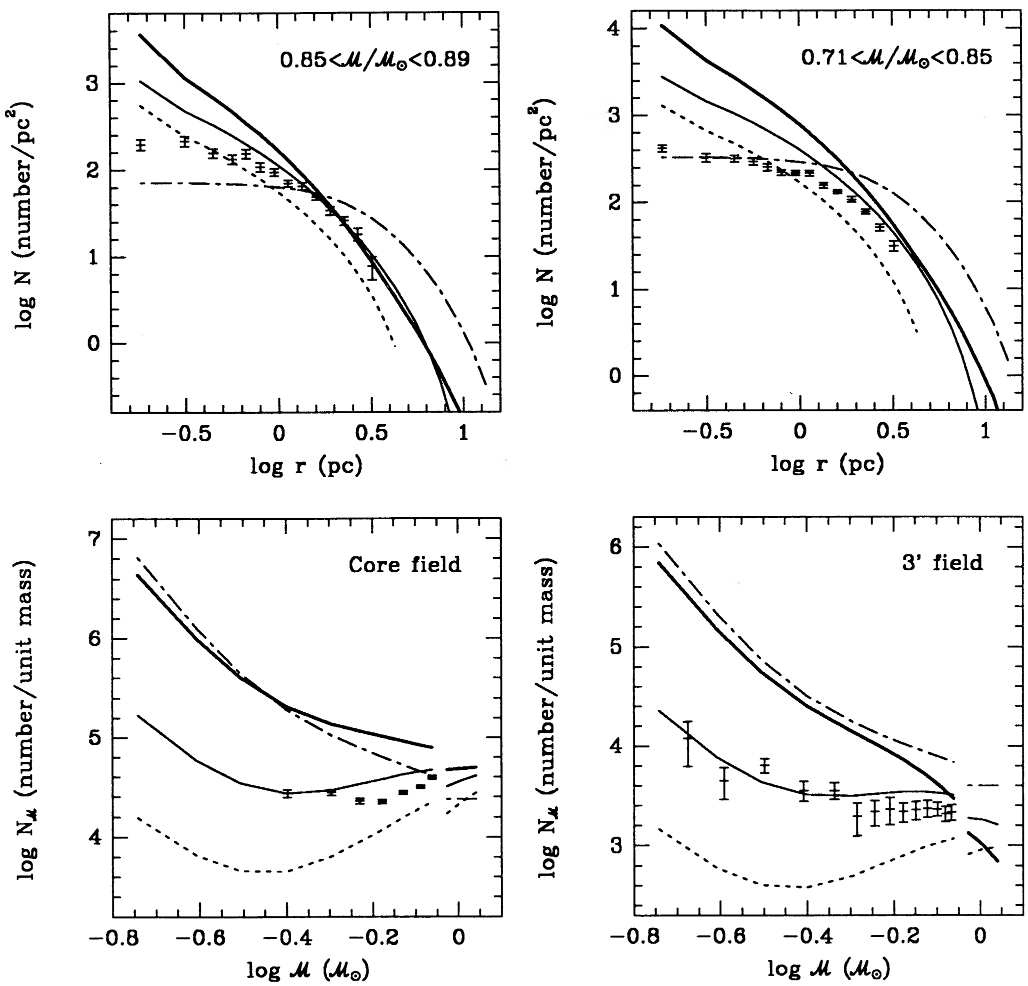

FIG. 3.—Our standard Fokker-Planck model compared to the observations at various times. The four panels refer to the two SDPs and two MFs of Figs. 1 and 2. The four times shown are initial King model (*dot-dash line*), at maximum core collapse (*heavy line*), the best fitting time when the mass is 10% of the initial mass (*thin solid line*), and when the mass is 3.5% of its initial value (*dashed line*).

collapse phase, the thin solid and dashed lines are for when the model has 10% and 3.5%, respectively, of its initial mass. The standard model best fits the outer SDPs (beyond ~1 pc) when the mass is 0.1 M_{initial} (*thin solid line*). The main problem in comparing the model to the observations is readily apparent in that the model SDPs at small radii are much steeper than those observed. The slope of the power-law section of the SDP does not flatten significantly during the entire post–core-collapse evolution. This behavior is common to all the models run with the exception of some of the special models to be discussed below. The model does not reproduce the detailed structure of the MFs, but the degree of mass segregation is similar to, although somewhat smaller than, that observed. A detailed match should not be expected until the SDP problem is resolved.

TABLE 2

INITIAL MASS FUNCTION

Mass ($M_\odot$)	Number Fraction	Mass Fraction
0.181..........	0.7118	0.5455
0.247..........	0.1403	0.1465
0.312..........	0.0488	0.0643
0.398..........	0.0390	0.0657
0.506..........	0.0162	0.0347
0.589..........	0.0102	0.0255
0.665..........	0.0085	0.0238
0.743..........	0.0073	0.0228
0.816..........	0.0052	0.0181
0.869..........	0.0027	0.0100
0.940..........	0.0033	0.0132
1.020..........	0.0033	0.0144
1.100..........	0.0033	0.0155

The tidal radius was chosen to give a good fit to the outer section of the SDP at the time in the evolution of the model that the model MFs had similar numbers as the observed MFs. The fits to the outer SDPs are not perfect; that observed for the more massive stars appears to be falling more quickly than the model profile. However, the model does give an estimate for the current tidal radius for M71 of about 10 pc. Since the length scale is a free parameter in the model, the SDP for the more massive stars was fit to the outermost seven data points to refine the estimate. The best fit gives a tidal radius of 9 pc. In the model, the tidal cutoff is applied in energy and is not instantaneous (the stripping rate is zero for stars with energies equal to that of the tidal limit), and so there will always be a population of unbound stars beyond the halo of the model.

Thus, unlike tidal radii based on King models, the tidal radii discussed here are not the distance at which the density goes to zero. For our models the zero-density radius is half again as large as the tidal radius. In the case of our standard model, the zero-density is 16 pc (14 pc if a detailed fit, as described above, is done). For the distance used here, the Kukarkin & Kireeva (1979) determination of the tidal radius of M71 is 15 pc. This is comparable with the zero-density radii based on the Fokker-Planck models.

The tidal radius estimated from the standard models seems quite robust. As will be discussed below, better fits to the SDPs (including the inner regions) were achieved using modifications to the standard model. The model with black holes discussed in § 5.2, and shown in Fig. 7, when fitted to the entire SDP of the more massive stars gives a tidal radius of 5.6 pc and a zero-density radius of 9 pc. The model with extra heating in § 5.3 (Fig. 9) gives radii of 9.3 pc and 14 pc (without fitting, $r_0 = 1$ pc) and 7 pc and 10 pc (best fit, $r_0 = 0.8$ pc) for the tidal and zero-density radii respectively.

A second set of estimates for the tidal radius of M71 are those based on the space velocity and distance modulus of Cudworth (1985). Given an assumed Galactic potential, the orbit of M71 within that potential can be calculated and the expected tidal radius computed. Ninković (1987) derives a tidal radius of 28–34 pc (depending on the Galactic potential used) for a tidal cutoff based on the perigalactic distance of the cluster's orbit. Allen & Martos (1988) estimate the tidal radius to be 25.2 pc using a similar technique but their own derivation of a Galactic potential. Both these studies and that of Kukarkin & Kireeva use the formula of King (1962) for the tidal radius and should be comparable with our zero-density radii. It has been argued (see, e.g., Keenan 1981 and Innanen, Harris, & Webbink 1983) that limiting radii based on this formula *overestimates* the true value by a factor of 3/2. Since similar assumptions regarding the nature of the tidal boundary have been made in all the estimates being considered here, we need not be concerned with such numerical factors. The problem is to understand why the estimates of the tidal radius based on the orbit of M71 are so much larger than those inferred from the distribution of stars in the cluster. Allen & Martos note that on theoretical grounds alone there is an uncertainty of at least a factor of 2 in their estimates of the tidal radii and the range of values given by Ninković indicate a similar uncertainty. On the other hand, none of the other clusters looked at by Allen & Martos have theoretical tidal radii as far off the observed value as is that of M71. Whether this is telling us that there is something genuinely different about M71 or not is unclear.

If M71 is in a post–core-collapse state, then the observed SDP shows too little central concentration compared with the standard models. Based on just the appearance of the surface brightness profile, and this has been the standard criterion, M71 is not considered to be a post–core-collapse cluster by Djorgovski & King (1986). Their determination is apparently based on the profile of Kron, Hewitt, & Wassermann (1984) in which the inner 0ʹ.7 were unusable for this purpose. Such an assumption was also made in RF89 and a reasonable fit to multimass King models was demonstrated. While the more detailed analysis of the RF89 data discussed above in § 2 suggests a small deviation from a King model profile, the significance of the result is uncertain. In any case, a "normal" King model profile does not necessarily say anything about the dynamical state of a cluster, although it is generally assumed that such a cluster is in a state well before core collapse. For M71 there are other observations which suggest a different story.

The present half-mass relaxation time of M71 is in the lower quartile of the observed distribution (see Fig. 8-2 of Binney & Tremaine 1987). The formula usually used for evaluating the half-mass relaxation time is that of Spitzer & Hart (1971):

$$t_{rh} = 0.138\left(\frac{Mr_h^3}{G}\right)^{1/2}\frac{1}{m\ln\Lambda}, \tag{1}$$

where M is the total mass, r_h, the half-mass radius, m, a mean mass, and $\ln\Lambda$, the usual Coulomb logarithm. If we use the observations of RF89, then, based on their discussion in § VI, we are seeing 95% of the light of the cluster and, further, if we assume that the mass-to-light ratio is constant with radius in the cluster (which is not the case due to mass segregation), then the half-mass radius is at 1.6 pc. Assuming that we are, in fact, seeing only half the mass of the cluster (the rest being too faint to see), then the total mass should be about $2 \times 10^4\ M_\odot$. This give a mass-to-light ratio of $M/L = 1.2$ in solar units. By way of comparison, Ninković (1987) adopted the mean M/L of 1.7 $M_\odot/L_\odot$ by Illingworth (1975) and derived a mass of 3×10^4 $M_\odot$. The mean mass of the stars counted by RF89 is $m = 0.626$ $M_\odot$. For the RF89 values, $t_{rh} = 1.1 \times 10^8$ yr. A similar estimate for the best-fitting model, when the model mass is 10% of the initial mass, where $M = 3 \times 10^4\ M_\odot$, $r_h = 2.1$ pc and $m = 0.52\ M_\odot$, yields $t_{rh} = 2.1 \times 10^8$ yr. Since equation (1) was originally derived for the case of relaxation where there are only stars of one mass present, it may be that a formula more appropriate to the multimass case will give a different result. Spitzer (1987), after giving the general form for a relaxation time in his equation (2-16),

$$t_r = \frac{v_m^3}{1.22n(4\pi G^2\langle m\rangle^2\ln\Lambda)}, \tag{2}$$

comments that if a system is near equipartition, a relaxation time for a multimass situation can be calculated using this equation if an appropriate mean mass and velocity dispersion are used. For the latter, he suggests using the mean kinetic energy per star divided by the mean mass. For a half-mass relaxation time, take n to be the mean density of stars within the half-mass radius and the mean kinetic energy to be the total kinetic energy, T, divided by the total number of stars. Then,

$$t_{rh} = 0.546\left(\frac{T}{M}\right)^{3/2}\frac{r_h^3}{N_h G^2\langle m\rangle^2\ln\Lambda}, \tag{3}$$

where N_h is the total number of stars within r_h. This form can be used only with models, where the total kinetic energy can be determined explicitly. For the standard model, which does approach equipartition in its inner regions at the late time under consideration, equation (3) gives $t_{rh} = 3.3 \times 10^8$ yr. These various estimates are consistent with a short relaxation time scale for M71. Multimass Fokker-Planck models have clearly shown that a pre–core-collapse cluster should reach core collapse after only a few half-mass relaxation times when a wide mass spectrum is present (see, e.g., Murphy & Cohn 1988). In fact, the standard model reached core collapse in only 2.9 of its initial half-mass relaxation times. One further comment on the model time scales. The amount of model time required for the standard model to evolve to the state which best fits the observations is about 30 Gyr, within a factor of 2 of the age of the stars in the cluster. It is difficult to predict on the basis of the input parameters whether a model as satisfactory as the standard model shown is possible on a more appropriate time scale, but at this point we do not regard the factor of two as a significant problem.

The Fokker-Planck simulations show that a pre–core-collapse model has a low degree of mass segregation and a fairly flat central SDP but will reach core collapse in only a few relaxation times. On the other hand, post–core-collapse models have very steep central SDPs and a high degree of mass segregation. The observed situation in M71 is that of a relatively flat SDP and strong mass segregation. We have two options. If, on the basis of the SDPs, we conclude that M71 is a pre–core-collapse cluster, then we are seeing the cluster at a special epoch, when it is on the verge of core collapse. Further, the mass segregation is unexplained unless we postulate that some of the mass segregation reflects initial conditions. However, the age of the stellar population of M71, like most of the Galactic globular clusters, is about 15 Gyr, so with its short relaxation time, a great deal of dynamical evolution must have already taken place, erasing the initial conditions. Attempts to find a pre–core-collapse model which fitted the observations were fruitless since, by the time sufficient mass segregation had taken place, the SDPs were already too steep. In order to consider M71 a pre–core-collapse cluster, we are forced to the conclusion that either we do not understand properly the time scales involved in two-body relaxation or we have failed to include some necessary physical processes.

The second option is to accept the mass segregation as indicating that M71 is a post–core-collapse cluster. In this case, since the cluster is expanding, the short relaxation time is not a problem. The agreement between the model and the observations can be taken as support for this option. The relatively flat observed SDPs, however, argue against M71's being post–core-collapse. In order to reconcile the observed and model SDPs in this case, additional physical processes are probably also required. Based on the models we see that no matter what we conclude about the evolutionary status of M71, there is a contradiction. Hence, if we are drawing the correct conclusions from the models and they are being properly applied, the observations are then telling us that there is something wrong with those models.

5. MODIFIED MODELS

In this section we will examine three possible adjustments to the standard model in attempting to resolve the contradictions between the Fokker-Planck models and the observations of M71.

5.1. *Gravothermal Oscillations*

The simplest thing to try is to modify the parameters controlling the numerical simulation. The nature of the behavior of a Fokker-Planck model is dependent on the size of the time step chosen. Cohn, Hut, & Wise (1989) have shown that as the time step length is decreased, the model goes from a smooth evolution into a chaotic state characterized by extreme fluctuations in central density. These gravothermal oscillations (GTOs) affect only the very central regions of the model, and it is as yet unclear whether they occur in real systems. Perhaps, then, we are observing M71 at the low density extreme of a GTO, and it is for this reason that the central cusp in the SDP is absent. Goodman (1987) showed that, in theory, GTOs will happen when the number of members of the cluster is sufficiently large. (See also Murphy et al. 1990 for discussion of gravothermal oscillations in multimass models and Cohn et al. 1991 for the chaotic nature of the oscillations.) If the cluster observations are sufficiently removed from the center of the cluster, or have insufficient spatial resolution to isolate the core, then the data should not depend significantly on the existence and amplitude of GTOs. All of the models described above have been calculated with a time step large enough to suppress the GTOs. In order to test the assumption that global properties are independent of GTOs, one run was restarted from several places with much smaller time steps and the results compared.

As may be seen in Figure 4, where the dotted line gives the evolution of the long time step run and the solid line that of the restarted runs with gravothermal oscillations, the global properties are, as expected, unaffected by the behavior of the core. The central values of density and velocity dispersion shown in Figure 4 are unphysical in the sense that they are evaluated from a statistical distribution at a radius corresponding to the presence of one star interior to it in projected density. Figure 5 shows a more realistic evaluation of these quantities, and the half-brightness radius with respect to the central density, by calculating averages over the inner 0.0178 pc (1″ at the distance of M71). The amplitude of the oscillations is much reduced, and the extreme excursions to high central densities are cut off by the limited spatial resolution. In Figure 6 we compare the model SDP at the extremes of its range for the earliest GTO run. For comparison, when the models of Murphy et al. (1990) reach their maximum expansion, the central flattening of the SDP only reaches out to 0.02 pc, about 1″ at the distance of M71. Certainly, over the radial region considered here, such small variations would be difficult to detect observationally and in any event are much too small to reduce the slope of the SDPs sufficiently to make them consistent with the observations. For most ground-based studies, gravothermal oscillations are less important in evaluating the SDPs of globular clusters. Recent *HST* results, which have resolved the core of M15 (Lauer et al. 1991), indicate that the effects of GTOs will have to be considered in these extreme cases.

5.2. *Modified IMFs*

We ran a series of models with a range of IMF slopes in an attempt to match the observed MFs. Some had one bin of 1.4 $M_{\odot}$ to represent the white dwarfs as opposed to the three, lower mass, white dwarf bins discussed above. Various slopes and combinations of slopes were tried ranging from -1 to 5. The relative proportions of degenerate and main-sequence stars was varied as well. We also ran a model similar to the standard one which had an extra low mass bin extending the mass function down to 0.1 $M_{\odot}$. This bin contained 58% of the cluster's mass and 80% of its stars, but the evolution of the core was not very different from the standard run. The main difference was that the model evolved somewhat faster, reaching core collapse in only 80% of the time required for the model without the extra, low-mass stars. In none of these cases was the power-law slope of the central part of the SDP small enough to be similar to that observed. From these tests we conclude that varying our basic IMF is not adequate.

Larson (1984) constructed two-component models based on simple assumptions regarding the form of the density and velocity dispersion profiles. Based on these, he could get fits to

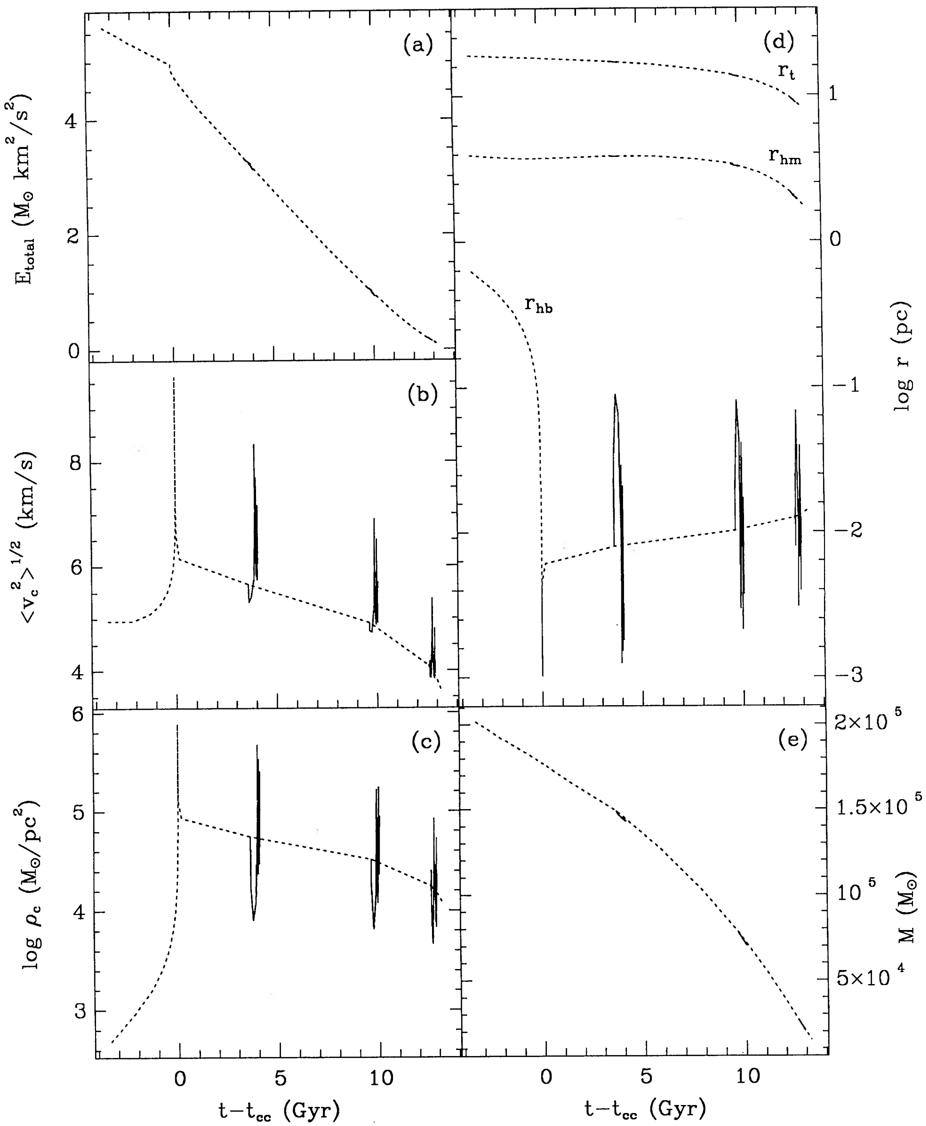

FIG. 4

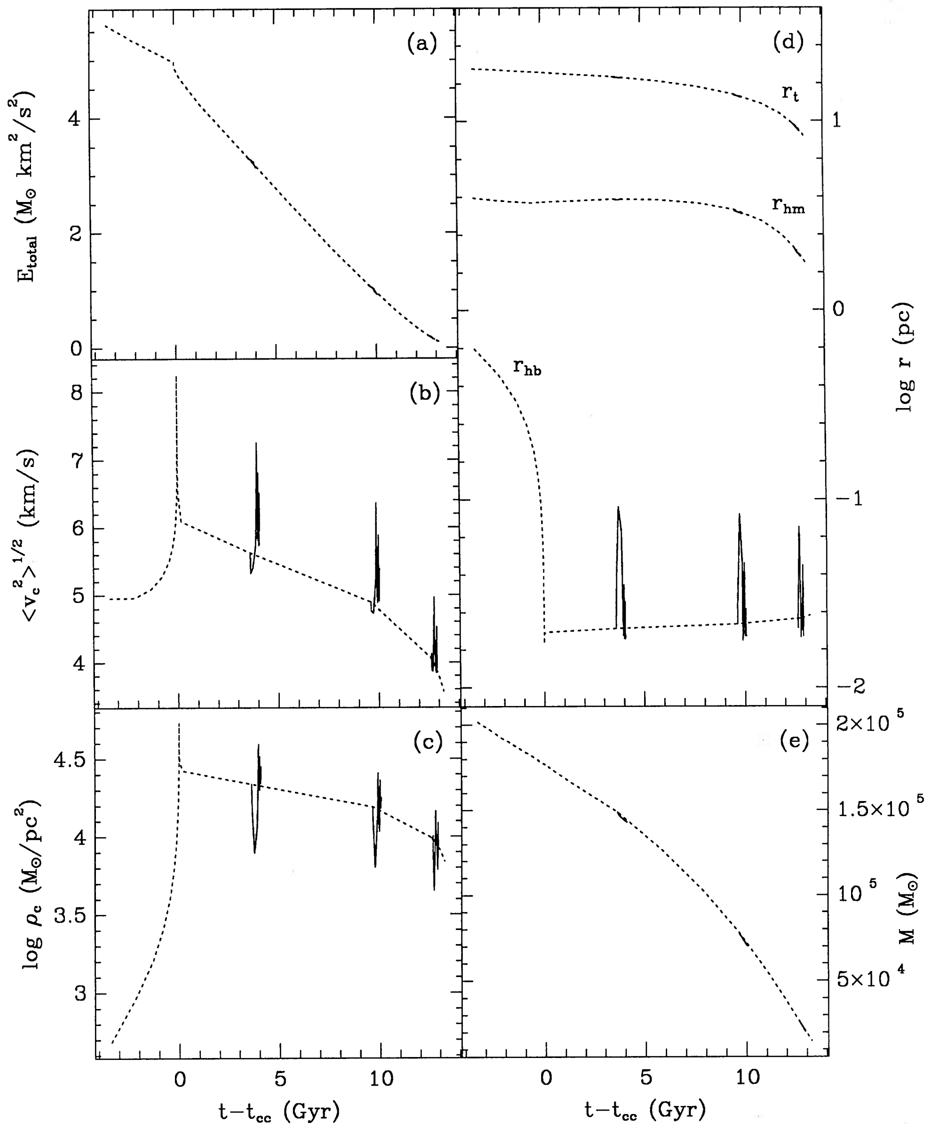

FIG. 5

FIG. 4.—A comparison of the evolution of a model when small time steps were used, allowing gravothermal oscillations to take place, with the evolution of the same model in which large time steps were used, suppressing the instability. The results from the long time step model are shown as dashed lines. The solid lines show the results obtained by restarting the smoothly varying model with smaller time steps at selected points in its evolution. The curves show (*a*) the total energy, E_{total}; (*b*) the central line-of-sight velocity dispersion, $\langle v_c^2 \rangle^{1/2}$; (*c*) the central density, ρ_c; (*d*) the tidal, r_t, half-mass, r_{hm}, and half-central-density radii, r_{hb}; and (*e*) the total mass, M. The density, velocity dispersion, and half-central-density radius are for the most massive stars dominating the cluster's light. Note how the global parameters (E_{total}, r_t, r_{hm}, M) are unaffected by the oscillations in the center of the model.

FIG. 5.—As Fig. 4, but the central density and velocity dispersions are averages over the inner arcsecond and the half-central-density radius is with respect to the averaged central density. The expanded ordinate scales should be noted when comparing this figure with the preceding one. The spatial averaging gives a more realistic prediction of the observable range for these quantities.

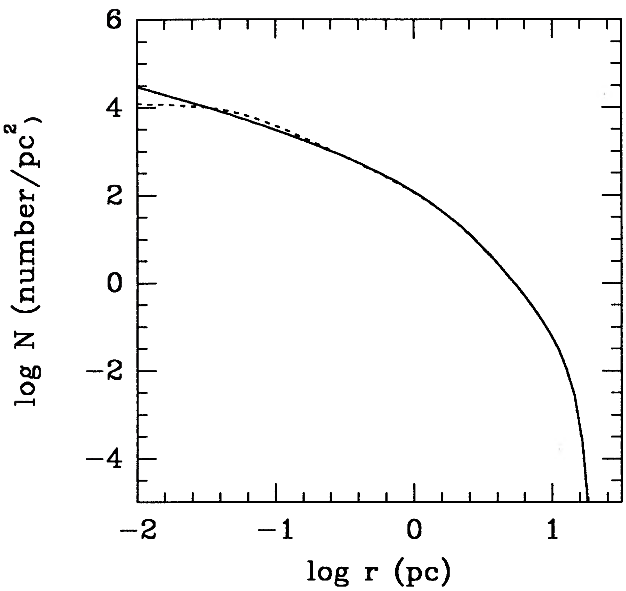

FIG. 6.—Surface density profiles for the bright stars at the two extremes of central density for the earliest set of oscillations in Fig. 4. The dashed line is the first minimum, and the solid line is the subsequent maximum. The difference would only be visible in the inner 2″ at the distance of M71.

the surface brightness profiles of several clusters by assuming a substantial fraction of dark, massive objects. His models indicated masses large enough that black holes were required. It is well established that a massive dark component, which will predominate in the core of the cluster due to mass segregation, will reduce the power-law slopes observed for less massive stars. The ratio of slopes is approximately proportional to the ratio of the masses of the stars given that the more massive class in fact dominates (see, for example, Chernoff & Weinberg 1990). To see if this would help resolve the M71 contradiction, we constructed a model with 3% of the initial mass in 2.5 $M_\odot$ "black holes."[1] Figure 7 shows the model at a late time when only 8% of the initial mass of 6×10^5 $M_\odot$ remained and some 40% of the current cluster mass was in the form of black holes.

For the more massive stars, the fit to the surface density profile is very good. The problem with this model lies in the degree of mass segregation between species and with radius. As can be seen in Figure 7 the shapes of the two model SDPs are nearly identical while Figure 1 shows that the SDP of the more massive stars is noticeably steeper than that of those less massive. This lack of mass segregation may be seen more clearly in the MFs. The model MFs are almost the same, allowing for the difference in absolute density, while the morphology of the observed MFs are quite different from each other. This case may seem somewhat extreme, but when we reduced the fraction of black holes the slope of the inner SDP became too steep very quickly while the degree of mass segregation was still insufficient to match the observations. Reducing the mass of the heavy component allows an increased degree of mass segregation but the mass ratio between the heavy component and the visible stars is then too small to provide sufficient flattening.

[1] No relativistic effects or destruction of stars by these massive objects were included in the model, so it is not quite accurate to refer to them as black holes. These effects might in fact be significant for cluster evolution but are beyond the scope of this paper.

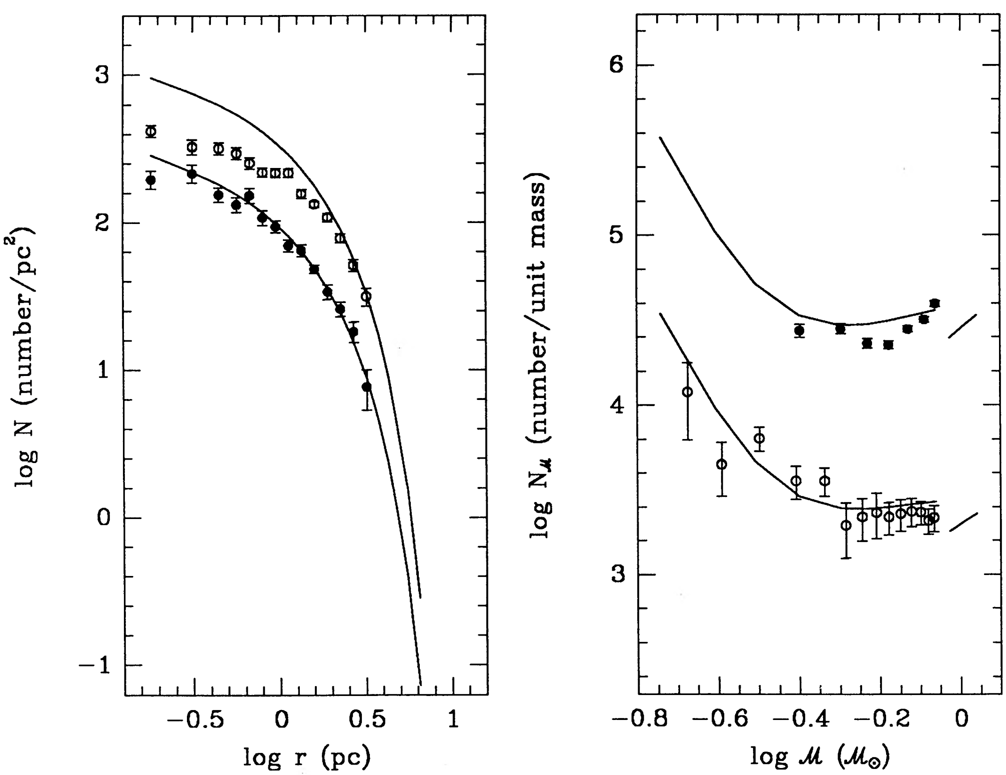

FIG. 7.—Comparison between the observations and model values for the run involving 3% by number of 2.5 $M_\odot$ black holes. Symbols for the data are as in Figs. 1 and 2. The curves shown are for the time when the model best fits the surface density profile for the more massive stars (*filled dots*).

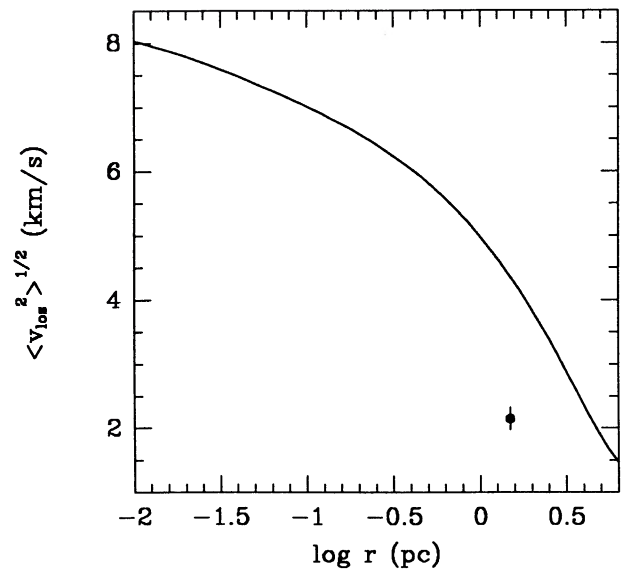

FIG. 8.—Line-of-sight velocity dispersion for the giants in the black hole model of Fig. 7. The point shows the measured value of Pryor (1990).

A further problem with the "black hole" hypothesis arises when the kinematics of the cluster star is considered. Pryor (1990) has measured the velocities of 79 members of M71 and gets a velocity dispersion of 2.15 ± 0.17 km s^{-1} at a mean radius of 1.5 pc. In our model, at the best-fitting time, the central velocity dispersion for this mass class is 8.2 km s^{-1} dropping to 2 km s^{-1} only at 4.5 pc as shown in Fig. 8. This observation appears to rule out the presence of a substantial, massive, dark component in the cluster.

5.3. *Heating*

The reheating source in these models is due to the statistical formation and destruction of three-body binaries. Following the discussion of Cohn et al. (1989), who adopt a heating rate based on the work of Hut (1985), we assumed that the amount of energy generated per binary formed was some 100 times the binding energy of the binary. If a more vigorous energy source is available to reverse core collapse, then shallower sloped SDPs are possible. We therefore ran a series of models with heating constants at various multiples of the standard one ranging from 10 to 10^6 times the energy input per binary.

As the heating rate was increased, the depth of core collapse decreased. Each model was checked against the observations

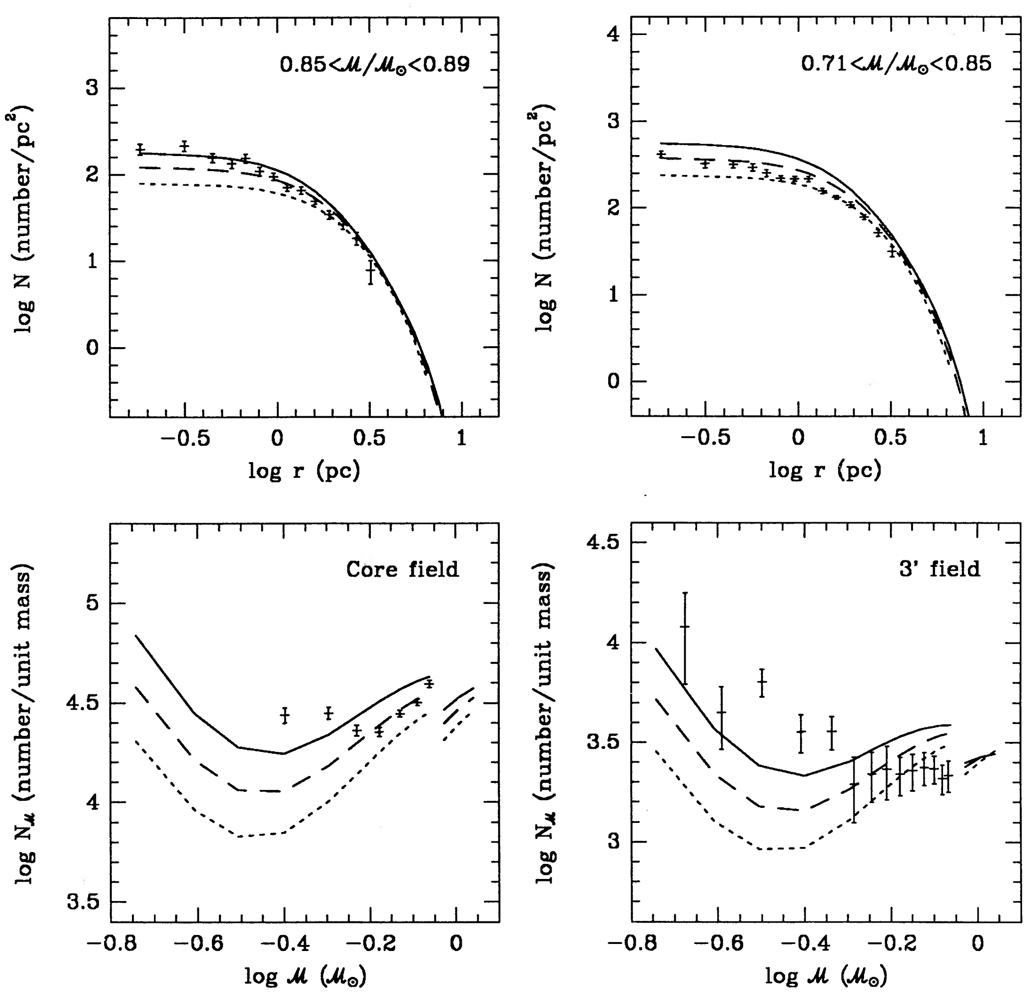

FIG. 9.—Comparison between the observations and model values for the run with the coefficient for binary heating set to 10^6 times that assumed in the standard model. The curves shown are for times when the mass is 7% (*solid*), 6% (*long dashed*), and 5% (*short dashed*) of the initial mass.

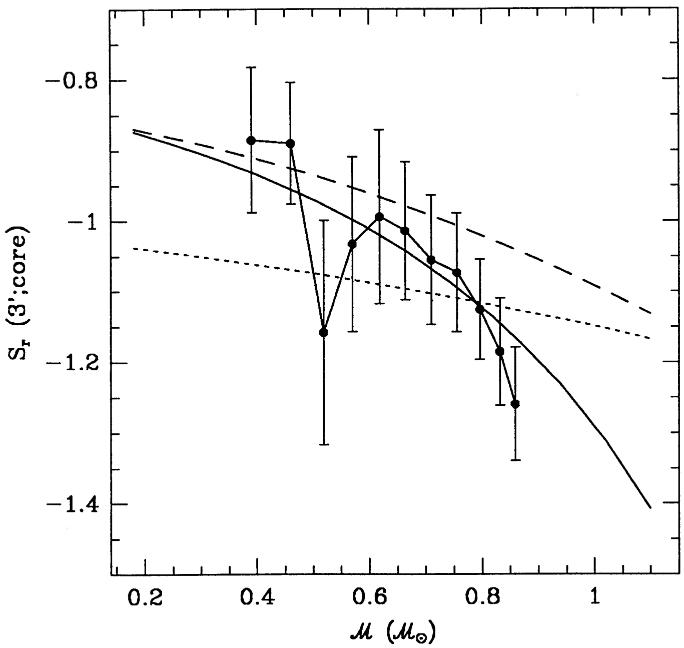

FIG. 10.—Segregation measures (see text) for the observed mass functions (*points*) and for the standard model of Fig. 3 (*solid line*), the model with black holes of Fig. 7 (*dotted line*), and the model with extra heating of Fig. 9 (*dashed line*).

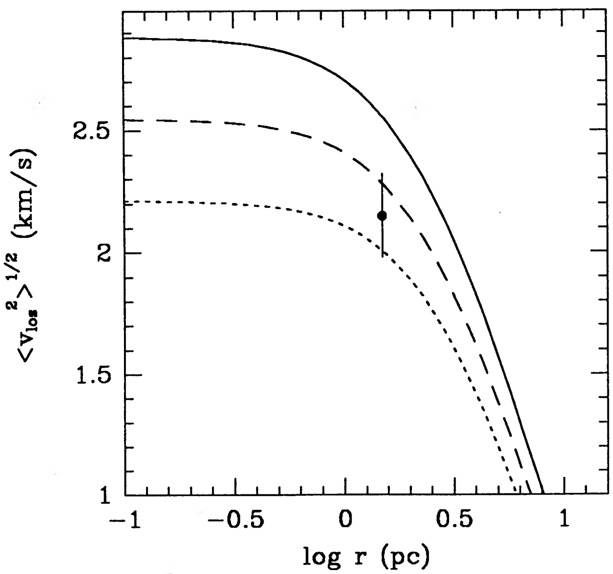

FIG. 11.—Line-of-sight velocity dispersion for the giants for the same model as in Fig. 9. The curves shown are for the same times as in that figure. The point is the measurement of Pryor (1990).

and only in the most extreme case, with a heating rate 10^6 times the standard value, was a good fit achieved. Figure 9 shows the results of this run. Both the SDPs are fitted well—if anything, the model SDPs are now insufficiently steep—although the model SDP for the less massive stars has somewhat too many stars at all radii. This can be accounted for with a slightly different IMF. The MFs, on the other hand, are not fitted as well, there being less mass segregation between the two fields than that observed.

In order to discuss the degree of mass segregation more quantitatively, we define a *segregation measure*, S, as the logarithm of the ratio of two mass functions. In this case we consider the segregation measure of the 3′ field with respect to the core field, but similar quantities could be defined for changes in the mass function with time (e.g., with respect to an IMF) or with space (e.g., with respect to a global mass function or a central mass function). Figure 10 shows the segregation measure $S_r = \log [N_M(3')/N_M(\mathrm{core})]$, where N_M is the number of stars per unit mass, for the observations and the three models shown in Figures 3, 7, and 9. From this diagram it is clear that the models with black holes and extra heating show insufficient mass segregation. The standard model compares much better with the observations, but even it may show insufficient mass segregation with respect to the observations. In each model where the segregation measure was calculated it was found to be a smooth, monotonic function of mass. Features such as the dip near 0.5 $M_\odot$ have never been seen. Considering the errors, this may not be a serious shortcoming. Figure 11 shows the projected velocity dispersion for the same times as Figure 9 together with the observed velocity dispersion of Pryor (1990). The model dispersions are consistent with the observation.

If the amount of heating driving the reexpansion of the cluster is the solution to the dilemma presented by M71, then there is a further problem in identifying the source of the extra heating. In these experiments the amount of heating has been parameterized in terms of the proportion of energy released by each binary formed. An energy release of 10^8 times the binding energy of the binary is an unphysical expectation. Even if we do not depend on the dynamical formation of binaries—for example if the presence of primordial binaries is important—the large amount of energy released per binary appears unreasonable.

However, it is important to note that the total energy released in the enhanced heating model is, in fact, slightly *less* than that released in the standard model. This result is illustrated in Figure 12, where the cumulative energy production is

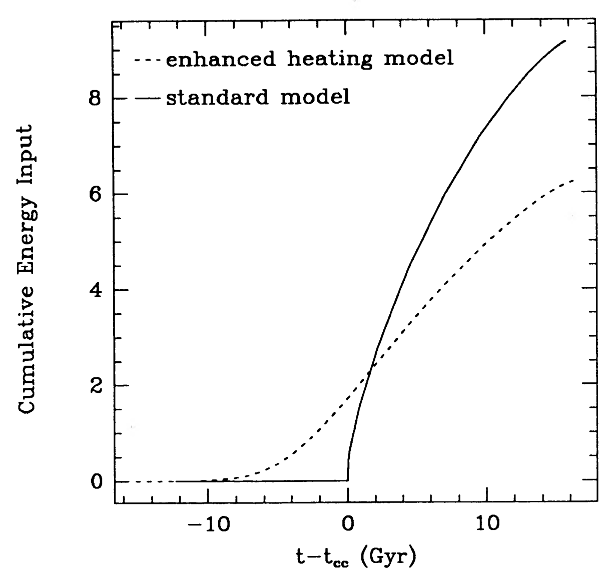

FIG. 12.—Cumulative energy production (in model units) vs. time for the standard model (*solid*) and the enhanced heating model (*dashed*). Despite the differences in the rate of energy production with time, the total energy produced in the cluster is about the same in both models.

plotted for the two models. In the standard model, the energy input is distributed as a short, sharp burst at core collapse followed by a long, lower level tail. This is easily understood because the binary heating essentially tracks the cube of the central density. As the standard model undergoes its deep core collapse, the heating rate rises very sharply, causing the cluster to quickly re-expand, thereby turning off the heating source. On the other hand, the model in which the energy released per binary has been enhanced does not suffer a deep core collapse, and the energy driving the reexpansion is distributed much more uniformly in time. The conclusion that may be drawn from this observation is that a continuous source of energy in a globular cluster will prevent a deep core collapse from taking place while still allowing for dynamical evolution. The cluster will still suffer from mass segregation, as some contraction of the core will take place, but the core densities will not reach the extremes expected in those models which require very high central densities to be achieved before enough energy can be released to reverse the contraction.

5.4. *Energy Sources*

The experiments with extra heating have led to a possible solution of the problem presented in M71. If we can include an energy source to supply the energy being transferred from the core to the halo, thus preventing extreme core collapse, while still allowing progress towards equipartition of energy and hence mass segregation, then a reasonable fit to clusters such as M71 may be possible. Arguments based on relaxation time scales such as those discussed above cannot then be used to determine the dynamical state of a cluster since two-body relaxation is no longer the only process occurring. The key to resolving the contradiction this way is to allow sufficient mass segregation, as observed, while preventing severe core collapse. What then are the candidates for additional energy sources?

Evidence is accumulating for the presence of primordial binary stars in globular clusters (Pryor et al. 1989). Gao et al. (1990) have run Fokker-Planck simulations which explicitly include a population of initial binaries along with one mass class of single stars. In these models the time to initial core collapse increases as the fraction of binaries increases. When 20% of the initial model is in binary stars, core collapse is delayed to 100 initial half-mass relaxation times. The effects of a population of primordial binaries on mass segregation cannot be estimated from the Gao et al. models. Much would depend on the mass distribution of the initial binary population. Goodman & Hut (1989), on theoretical grounds, suggest that, depending on the initial abundance of binaries and their rate of destruction, the presence of primordial binaries would result in a relatively large core and hence a SDP which does not show a cusp. On the other hand, such a core is likely to consist mostly of binaries. Core collapse in the models of Gao et al. terminates when the mass segregation between the binaries and singles is complete, again with a core dominated by binaries. The high binary fraction expected in the core is thus a testable prediction of this scenario. The presence of a large number of blue stragglers in the core of M71 (Richer & Fahlman 1988) is suggestive, but the overall binary frequency in the cluster center remains unknown.

A second, and unquestionably significant, energy source is that due to stellar evolution. Chernoff & Weinberg (1990) discuss an extensive series of pre–core-collapse models which include stellar evolution in addition to a tidal boundary condition. With their initial conditions, models which do not start out sufficiently concentrated are disrupted due to stellar evolution before any dynamical evolution takes place. A steep IMF having only a small number of massive stars aids in holding the cluster together against the heating effects of stellar mass loss. The applicability of these models to real clusters is problematic in that the mass function only includes stars more massive than 0.4 $M_{\odot}$. The deep mass functions presented for several clusters by Richer et al. (1990) clearly show the presence of a large number of stars with masses below this limit. In the case of NGC 6397 the mass function approaches the hydrogen-burning limit without any sign of turning over (Fahlman et al. 1989). The effect of including an extended low-mass tail to the IMF should have similar stabilizing effects as using a steeper IMF slope. Applegate (1986) used simple models to show that clusters will be supported against core collapse so long as the stellar evolution time scale of the most massive remaining species is several relaxation times. Since the relaxation time is increased by the effects of mass loss, core collapse may be postponed indefinitely for a sufficiently flat IMF. It is possible that in some clusters, depending on the details of their structure, this will serve to support the cluster against collapse while still allowing mass segregation to take place. Unfortunately, the models presented by Chernoff & Weinberg (1990) do not appear to show such a case of a cluster temporarily held between core collapse and evaporation and it may require fine tuning to produce one. A cluster wherein this epoch ended shortly before the present would now appear to be approaching core collapse. This scenario will need to be modeled in detail to see if the solution to the problem of M71 lies here.

5.5. *Beyond Fokker-Planck Models*

Until now all the proposed solutions to the dilemma posed by M71 have been within the framework of present-day Fokker-Planck models. The assumptions underlying the orbit-averaged Fokker-Planck equation prevent us from including any effects occurring on time scales shorter than the dynamical time scale or those which operate in a non–spherically symmetric manner. Based on the space velocity of Cudworth (1985), Ninković (1987) finds that M71's orbit lies in the disk of the galaxy with an inclination of 172°. With such an orbit, it is subject to many effects not included, or includable in these models such as tidal shocks due to disk passages, bulge passages, and interactions with giant molecular clouds. Tidal shocks due to disk passages, for example, which are usually treated in an impulse approximation, violate both assumptions. We have treated the tidal stripping surface here as spherical, a necessary simplification. In reality however, the surface is more complicated. Preferential stripping of stars on low angular momentum orbits may cause the velocity dispersion to be anisotropic. If physical processes such as these are needed to resolve the problems discussed here, then another approach, such as full N-body calculations (McMillan, Hut, & Makino 1990 show the beginnings of such an approach), will be required.

6. SUMMARY

Our attempt to use an orbit-averaged Fokker-Planck code which includes a mass spectrum, simple tidal stripping, and a statistical treatment of a three-body binary heating source to find a model which matches the observed SDPs and MFs for M71 has uncovered a contradiction. The presence of a high degree of mass segregation and an apparently short relaxation time suggest that M71 is a highly evolved cluster. Any model with such characteristics is either suffering core collapse or is in the post–core-collapse phase of its evolution. These same models, however, also have steep, power-law SDPs in their central regions. This contradicts the observed SDPs for M71 which are only somewhat more concentrated than a King model, certainly not the steep power laws predicted. It was found that while modifying the IMF does not help in solving the problem, a large increase in the heating rate can give models approximating the observations. It is suggested then that additional heat sources, which are not necessarily dependent on the high central densities reached at core collapse, are present in globular clusters and support them against core collapse. Under this interpretation, clusters such as M71 are not in fact post–core-collapse systems, while still showing dynamical evolution. As well, it may be that processes which cannot be included in the orbit-averaged Fokker-Planck formulation are important in the evolution of globular clusters. In either case, the problem of M71 demonstrates that a Fokker-Planck code of the type used here is inadequate for modeling all globular clusters. The most promising line of inquiry is to include changes in the mass spectrum due to stellar evolution, a point we will return to in a future paper.

This research has been supported in part by the Natural Sciences and Engineering Research Council of Canada and by an I. W. Killam Fellowship to G. A. D.

APPENDIX

THE THREE-BODY HEATING TERM

With respect to the choice of form for the three-body heating term, there are two expressions in use based on suggestions by D. Heggie and P. Hut. The first is that of Murphy, Cohn, & Hut (1990, hereafter MCH), and the second is that of LFR, which is used here. Both groups use the same form for the Fokker-Planck equation and their computer codes are both descendants of the original code of Cohn (1980). In these, the distribution functions are functions of energy per unit mass. The heating rate is given by the rate at which binaries are created in the given conditions of the cluster, multiplied by the energy contributed to the cluster by each binary. The total heating rate is then to be distributed to each species in proportion to their relative densities, i.e.,

$$\dot{E}_i = \frac{\rho_i}{\rho}\,\dot{E}_{\rm total}\,. \tag{A1}$$

The details differ in the two cases and will be dealt with in turn.

LFR start with a heating rate per unit volume, assuming that the energy released per binary is proportional to the density-weighted, central velocity dispersion v_c^2. In their formulation

$$\dot{E}^{\rm L}_{\rm total} = C_{\rm L}\,G^5 v_c^2\left(\sum_i \rho_i m_i v_i^{-3}\right)^3 . \tag{A2}$$

We require a heating rate per unit mass to be dimensionally consistent with the Fokker-Planck equation, so we divide $\dot{E}^{\rm L}_{\rm total}$ by ρ, the total density, and orbit-average the result to give the heating coefficient. If we designate the sum in equation (A2) by $S_{\rm L}$ then the heating coefficient is

$$H^{\rm L}(E) = 16\pi^2 C_{\rm L}\,G^5 v_c^2 \int_0^{\phi^{-1}(E)} [2(\phi(r) - E)]^{1/2}\,\frac{S_{\rm L}^3(r)}{\rho(r)}\,r^2\,dr \tag{A3}$$

for all species. The total change in energy for each species is given by

$$\begin{aligned}
\Delta E_i^{\rm L} &= m_i \int_0^{\phi(0)} H^{\rm L} f_i\,dE \\
&= 16\pi^2 C_{\rm L}\,G^5 v_c^2 m_i \int_0^{\phi(0)} f_i \int_0^{\phi^{-1}(E)} [2(\phi - E)]^{1/2}\,\frac{S_{\rm L}^3}{\rho}\,r^2\,dr\,dE \\
&= 16\pi^2 C_{\rm L}\,G^5 v_c^2 m_i \int_0^{\phi^{-1}(0)} \frac{S_{\rm L}^3}{\rho}\,r^2 \int_0^{\phi(r)} f_i[2(\phi - E)]^{1/2}\,dE\,dr \\
&= 4\pi C_{\rm L}\,G^5 v_c^2 \int_0^{\phi^{-1}(0)} S_{\rm L}^3\,\frac{\rho_i}{\rho}\,r^2\,dr \\
&= 4\pi \int_0^{\phi^{-1}(0)} \frac{\rho_i}{\rho}\,\dot{E}^{\rm L}_{\rm total}\,r^2\,dr \\
&= 4\pi \int_0^{\phi^{-1}(0)} \dot{E}_i^{\rm L} r^2\,dr
\end{aligned} \tag{A4}$$

as desired.

MCH use a heating rate per particle of the form

$$\dot{E}^{\rm M}_{\rm total} = C_{\rm M}\, G^5 \left(\sum_i n_i^{2/3} m_i^2 v_i^{-7/3} \right)^3 . \tag{A5}$$

MCH use a heating coefficient for species i of the form

$$H_i^{\rm M}(E) = 16\pi^2 C_{\rm M}\, G^5 \left[\frac{m_i f_i(E)}{\sum m_i f_i(E)} \right] \int_0^{\phi^{-1}(E)} [2(\phi - E)]^{1/2} S_{\rm M}^3 r^2\, dr , \tag{A6}$$

where $S_{\rm M}$ is the sum in equation (A5). Note that $H_i^{\rm M}$, as written here and in MCH, is dimensionally inconsistent with the Fokker-Planck equation, because of an extra dimension of mass. We may calculate the total heating for each species, as above:

$$\begin{aligned} \Delta E_i^{\rm M} &= \int_0^{\phi(0)} H_i^{\rm M} f_i\, dE \\ &= 16\pi^2 C_{\rm M}\, G^5 \int_0^{\phi(0)} f_i \left(\frac{m_i f_i}{\sum m_i f_i} \right) \int_0^{\phi^{-1}(r)} [2(\phi - E)]^{1/2} S_{\rm M}^3 r^2\, dr\, dE \\ &= 16\pi^2 C_{\rm M}\, G^5 m_i \int_0^{\phi^{-1}(0)} S_{\rm M}^3 r^2 \int_0^{\phi(r)} \frac{f_i^2}{\sum m_i f_i} [2(\phi - E)]^{1/2}\, dE\, dr \end{aligned} \tag{A7}$$

which, clearly does not reduce to an expression involving the total energy rate weighted by the density fractions. MCH state that "each species receives an amount of energy in its energy bin, E, according to the orbit average of equation (3) [eq. (A5) above], per unit time, multiplied by its fractional density" as in equation (A1). Since the orbit average of equation (A5) (eq. [A6] apart from the weighting factor involving $m_i f_i$) is now in energy space, MCH cannot simply multiply it by the fractional densities, since these are in radial coordinates, and, hence, are forced into the approximation of using the fractional distribution function instead.

A comparison between the models of MCH and similar models calculated here indicates that the difference in the adopted expressions for the heating rate has no apparent effect on the results. Due to mass segregation, the core is dominated by the most massive stars and in the single species limit the two expressions are equivalent. In view of the consistency argument, and the reduced requirements for data storage and computational time, the formalism adopted here for calculating the heating coefficient, i.e., equation (A3), is to be preferred.

REFERENCES

Allen, C., & Martos, M. A. 1988, Rev. Mexicana Astron. Af., 16, 13
Applegate, J. 1986, ApJ, 301, 132
Binney, J., & Tremaine, S. 1987, Galactic Dynamics (Princeton: Princeton Univ. Press)
Chernoff, D. F., & Weinberg, M. D. 1990, ApJ, 351, 121
Cohn, H. 1979, ApJ, 234, 1036
———. 1980, ApJ, 242, 765
Cohn, H., Hut, P., & Wise, M. 1989, ApJ, 342, 814
Cohn, H., Lugger, P. M., Grabhorn, R. P., Breedan, J. L., Packard, N. H., Murphy, B. W., & Hut, P. 1991, in The Formation and Evolution of Star Clusters, ed. K. Janes (ASP Conf. Ser., 13), 381
Cudworth, K. M. 1985, AJ, 90, 65
Djorgovski, S. G., & King, I. R. 1986, ApJ, 305, L61
Elson, R., Hut, P., & Inagaki, S. 1987, ARA&A, 25, 565
Fahlman, G. G., Richer, H. B., Searle, L., & Thompson, I. B. 1989, ApJ, 343, L49
Gao, B., Goodman, J., Cohn, H., & Murphy, B. 1991, ApJ, 370, 567
Goodman, J. 1987, ApJ, 313, 576
Goodman, J., & Hut, P. 1989, Nature, 339, 40
Grabhorn, R. P., Cohn, H. N., Lugger, P. M., & Murphy, B. W. 1991, in The Formation and Evolution of Star Clusters, ed. K. Janes (ASP Conf. Ser., 13), 392
Hut, P. 1985, in IAU Symp. 113, The Dynamics of Star Clusters, ed. J. Goodman & P. Hut (Dordrecht: Reidel), 231
Illingworth, G. 1975, in IAU Symp. 69, Dynamics of Stellar Systems, ed. A. Hayli (Dordrecht: Reidel), 151
Innanen, K. A., Harris, W. E., & Webbink, R. F. 1983, AJ, 88, 338
Keenan, D. W. 1981, A&A, 95, 340
King, I. 1962, AJ, 67, 471
———. 1966, AJ, 71, 64
Kron, G. E., Hewitt, A. V., & Wassermann, L. H. 1984, PASP, 96, 198
Kukarkin, B. V., & Kireeva, N. N. 1979, Soviet Astron., 23, 261
Larson, D. 1984, MNRAS, 210, 763
Lauer, T. R., et al. 1991, ApJ, 369, L45
Lee, H. M. 1987, ApJ, 319, 801
Lee, H. M., Fahlman, G. G., & Richer, H. B. 1991, ApJ, 366, 455 (LFR)
Lee, H. M., & Ostriker, J. P. 1987, ApJ, 322, 123
McMillan, S., Hut, P., & Makino, J. 1990, ApJ, 362, 522
Murphy, B. W., & Cohn, H. 1988, MNRAS, 232, 835
Murphy, B. W., Cohn, H., & Hut, P. 1990, MNRAS, 245, 335 (MCH)
Ninković, S. 1987, Bull. Astron. Inst. Czechoslovakia, 38, 147
Pryor, C. 1990, private communication
Pryor, C., McClure, R. D., Hesser, J. E., & Fletcher, J. M. 1989, in Dynamics of Dense Stellar Systems, ed. D. Merritt (Cambridge: Cambridge Univ. Press), 175
Richer, H. B., & Fahlman, G. G. 1988, ApJ, 325, 218
———. 1989, ApJ, 339, 178 (RF89)
Richer, H. B., Fahlman, G. G., Buonanno, R., & Fusi Pecci, F. 1990, ApJ, 359, L11
Shawl, S. J., & White, R. E. 1986, AJ, 91, 312
Spitzer, L. 1987, Dynamical Evolution of Globular Clusters (Princeton: Princeton Univ. Press)
Spitzer, L., & Hart, M. H. 1971, ApJ, 164, 399